[COL778] Assignment 1: State Estimation

Hemanshu Garg — 2022CS11090

Drive link to plots: `https://drive.google.com/drive/folders/1zTyv191DxiWzj3126SqeRf8om2Qtnppt?usp=sharing`

Part I - 1D State Estimation

(a) Motion and Observation Models

We define the state vector as

$$\mathbf{x}_t = \begin{bmatrix} x_t \\ \dot{x}_t \end{bmatrix},$$

and the **Motion Model** is given by

$$\mathbf{x}_t = A_t\,\mathbf{x}_{t-1} + B_t\,u_t + \boldsymbol{\epsilon}_t,$$

where $\boldsymbol{\epsilon}_t \sim \mathcal{N}(0, R)$ represents the process noise and the control policy u_t is defined as

$$u(t) = \begin{cases} 400, & \text{if } t < 0.25, \\ -400, & \text{if } 3 < t < 3.25, \\ 0, & \text{otherwise.} \end{cases}$$

The matrices A_t and B_t are defined as follows:

$$A_t = \begin{bmatrix} 1 & \Delta t \\ 0 & 1 \end{bmatrix}, \qquad B_t = \begin{bmatrix} \frac{1}{2}\Delta t^2 \\ \Delta t \end{bmatrix}.$$

Observation Model: We assume that the measurements are obtained via the observation model:

$$z_t = C_t\,\mathbf{x}_t + \delta_t,$$

where C_t is the observation matrix and $\delta_t \sim \mathcal{N}(0, Q)$ represents the measurement noise. The observation matrix is defined based on

$$C_t = \begin{bmatrix} \frac{2}{v_{\text{sound}}} & 0 \end{bmatrix}.$$

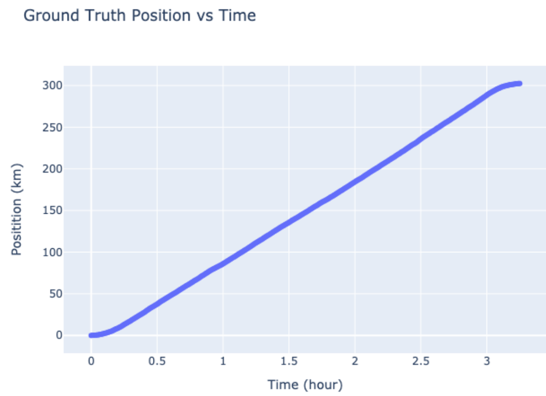

Figure 1: Simulated ground truth position versus time.

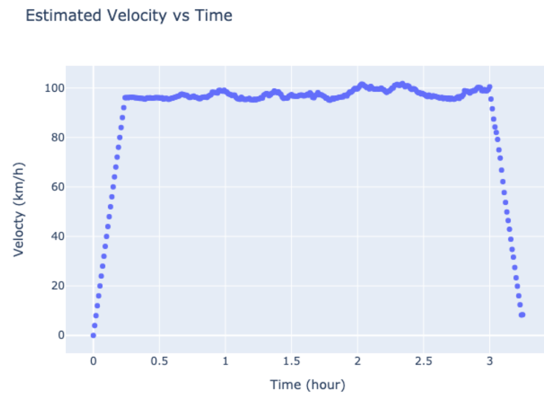

Figure 2: Simulated ground truth velocity versus time.

(b) Kalman Filter

At each time step t, the Kalman filter produces an estimate of the state μ_t and the associated error covariance Σ_t.

Prediction Step: Given the estimate μ_{t-1} with covariance Σ_{t-1} at time $t-1$, the predicted state and covariance are computed as

$$\mu_{t|t-1} = A_t\,\mu_{t-1} + B_t\,u_t,$$

$$\Sigma_{t|t-1} = A_t\,\Sigma_{t-1}\,A_t^\top + Q,$$

where Q is the process noise covariance.

Update Step: When a measurement z_t is available, with measurement matrix C_t and measurement noise covariance R, the Kalman gain K_t is computed as

$$K_t = \Sigma_{t|t-1}\,C_t^\top \left(C_t\,\Sigma_{t|t-1}\,C_t^\top + R\right)^{-1}.$$

The state estimate and covariance are then updated using

$$\mu_t = \mu_{t|t-1} + K_t\left(z_t - C_t\,\mu_{t|t-1}\right),$$

$$\Sigma_t = (I - K_t\,C_t)\,\Sigma_{t|t-1}.$$

This recursive procedure provides an optimal estimate (in the minimum mean-square error sense) of the train state at each time step.

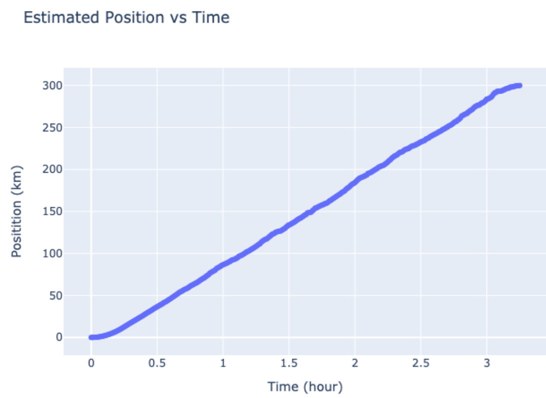

Figure 3: Estimated position versus time using the Kalman filter.

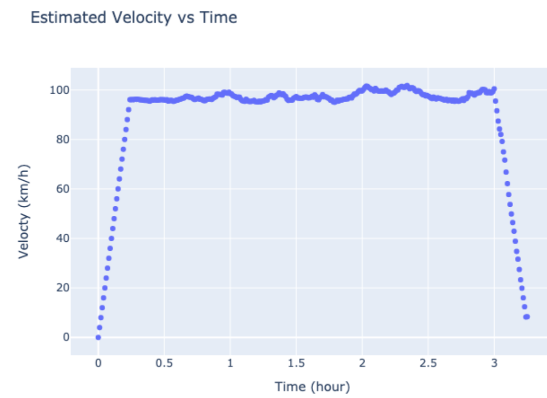

Figure 4: Estimated velocity versus time using the Kalman filter.

(c) Joint Plot of Actual and Estimated Trajectory with Uncertainty Bars

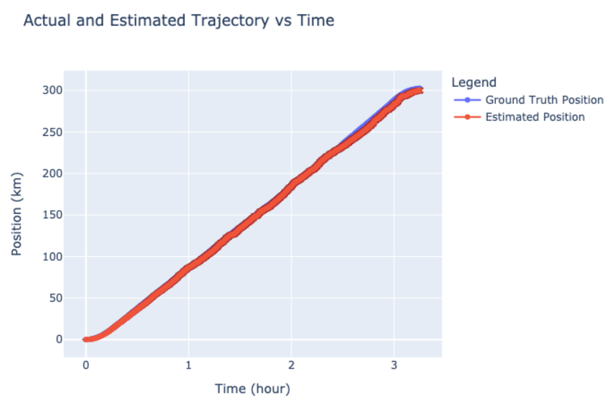

Figure 5: Actual and estimated position trajectory with uncertainty bars.

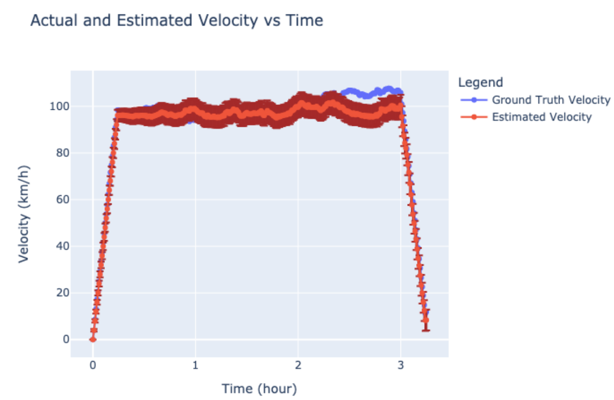

Figure 6: Actual and estimated velocity trajectory with uncertainty bars.

- The estimated position follows the ground truth well with small uncertainty bars.
- Velocity estimates are more off compared to ground truth and also uncertainty bars are larger.
- This is happening because we are only measure position in our z_t and for velocity updates we are relying only on correlations from motion model.

(d) Varying Noise Parameters

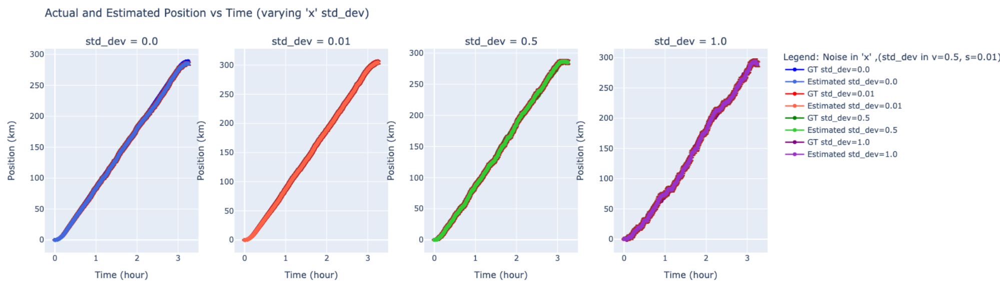

Figure 7: Position versus time for varying position noise standard deviation.

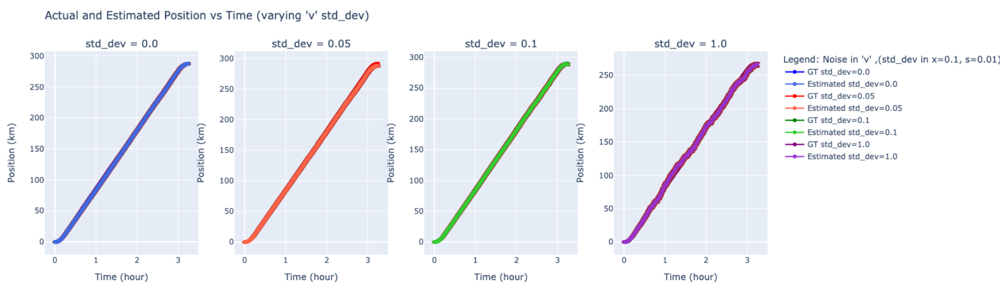

Figure 8: Position versus time for varying velocity noise standard deviation.

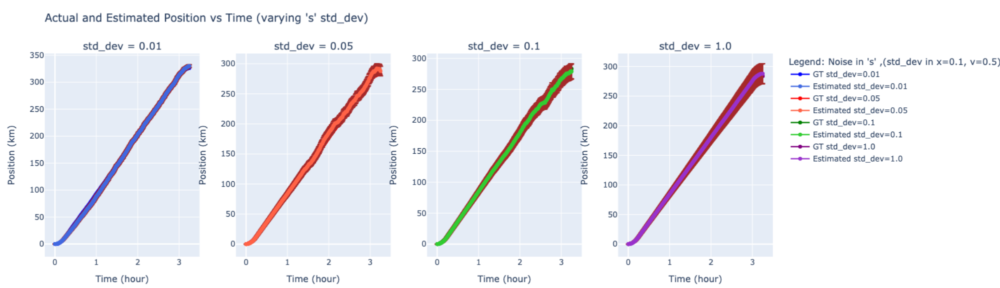

Figure 9: Position versus time for varying sensor noise standard deviation.

Observations

- When position noise is increased position of the train itself is does not increase smoothly (our acceleration being transfered non uniformly and introducing jerks).
- When velocity noise is increased position again gains randomness which makes sense as position is related to velocity according to motoin model.
- in both cases uncertainty bars of estimates increase with increasing noise.
- When sensor noise is increased the the uncertainty bars become larger and also increase over time for large noise, which make sense as once our measurements become less reliable beyond a point our updates will keep increasing the spread in our belief as corrections are not able to sufficiently compensate.

(e) Analysing Kalman Gain by Varying Noise

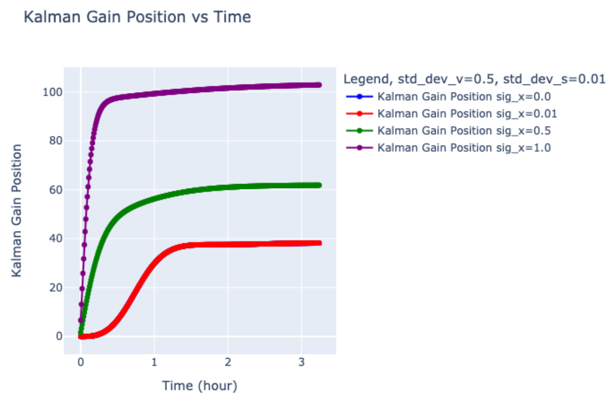

Figure 10: Kalman gain for position estimates with varying position noise standard deviation.

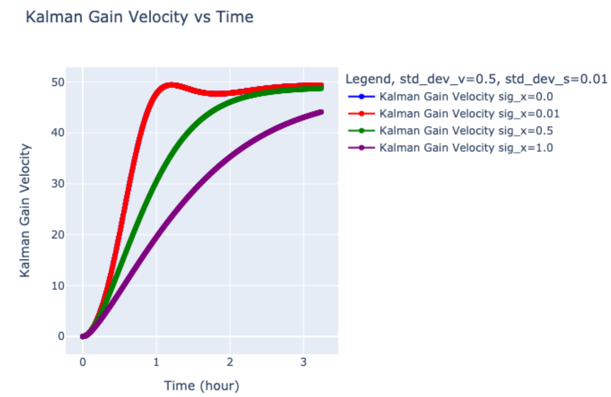

Figure 11: Kalman gain for velocity estimates with varying position noise standard deviation.

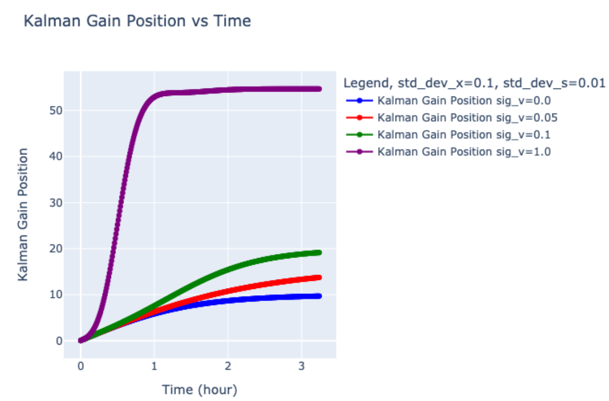

Figure 12: Kalman gain for position estimates with varying velocity noise standard deviation.

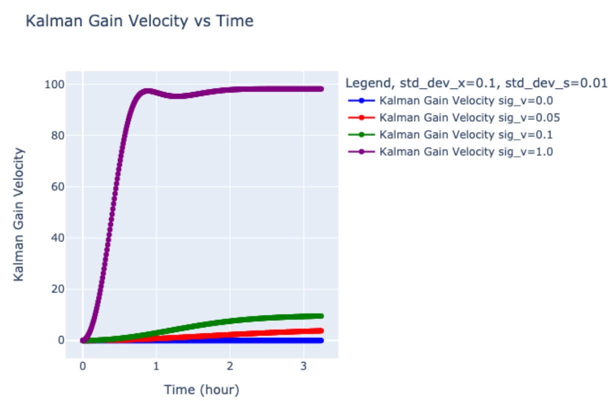

Figure 13: Kalman gain for velocity estimates with varying velocity noise standard deviation.

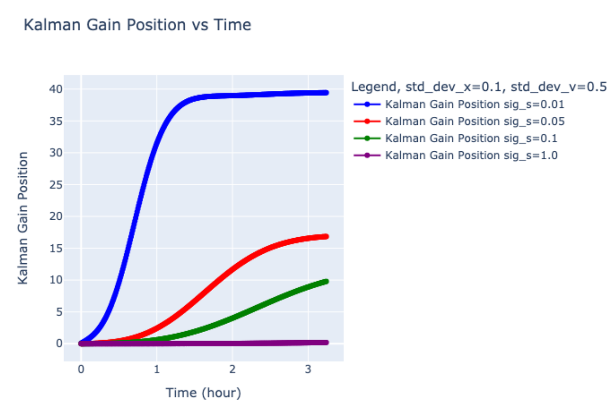

Figure 14: Kalman gain for position estimates with varying sensor noise standard deviation.

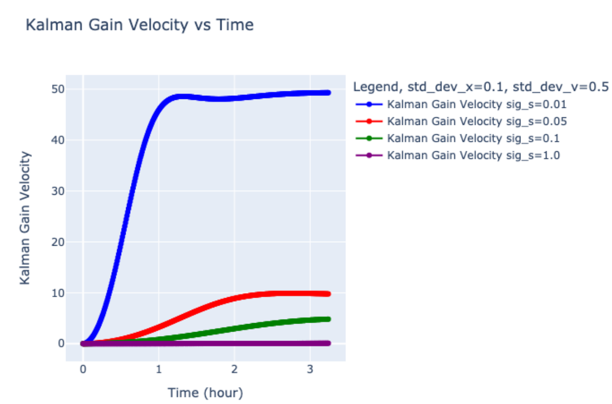

Figure 15: Kalman gain for velocity estimates with varying sensor noise standard deviation.

Interpretation of Kalman gain: It tell about how much we trust our measurements and how to quantitatively weigh our corrections from measurements.

- **Process Noise:**
  - Increasing process noise (either in position or velocity) leads to a larger predicted uncertainty in position. This causes the Kalman gain for the **position** to increase (i.e., the filter corrects the position estimate more strongly).
  - However, higher process noise in position reduces the kalman gain in velocity, this is due to mathematically σ_{xx} coming in denominator for velocity kalman gain, can be interpreted as decoupling of position and velocity.
- **Sensor Noise:** Increasing sensor noise results in a decrease in both the position and velocity Kalman gains, meaning that the filter will rely more on its prediction than on the noisy measurements.

(f) Filtering under Partial Observations

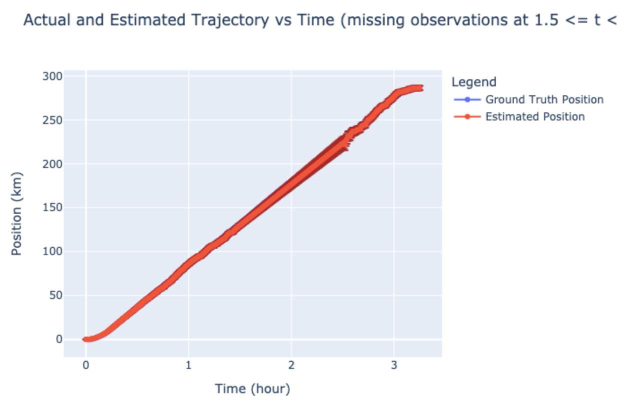

Figure 16: Actual and estimated position trajectory under partial observations.

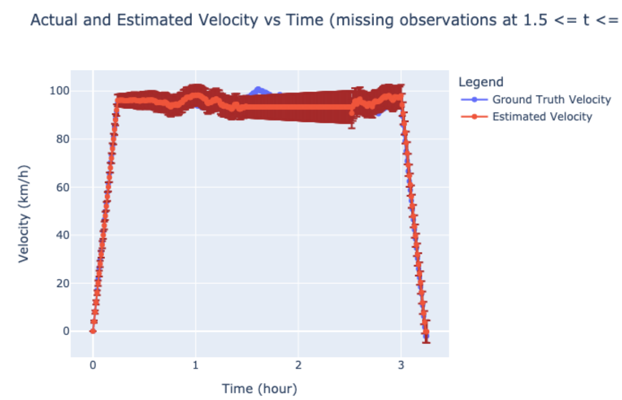

Figure 17: Actual and estimated velocity under partial observations.

Observations:
We see that uncertainty bars(indicated by brown bars) increase in size the region of of time between 1.5 and 2, which makes sense as our updates in belief is only through past data which will increase our uncertainty and once observations start coming through again uncertainty bars shrink.

Part II: State Estimation in 3D

In this problem, the state of the football at time t is given by

$$\mathbf{X}_t = \begin{bmatrix} x_t \\ y_t \\ z_t \\ \dot{x}_t \\ \dot{y}_t \\ \dot{z}_t \end{bmatrix}.$$

(a) Motion Model and Observation Models

Motion Model: The evolution of the state is modeled by a discrete-time linear system:

$$\mathbf{X}_t = A_t\,\mathbf{X}_{t-1} + B_t\,u_t + \boldsymbol{\epsilon}_t,$$

where:

- A_t is the state transition matrix:

$$A_t = \begin{bmatrix} 1 & 0 & 0 & \Delta t & 0 & 0 \\ 0 & 1 & 0 & 0 & \Delta t & 0 \\ 0 & 0 & 1 & 0 & 0 & \Delta t \\ 0 & 0 & 0 & 1 & 0 & 0 \\ 0 & 0 & 0 & 0 & 1 & 0 \\ 0 & 0 & 0 & 0 & 0 & 1 \end{bmatrix};$$

- B_t is the control input matrix:

$$B_t = \begin{bmatrix} 0 \\ 0 \\ \frac{1}{2}\Delta t^2 \\ 0 \\ 0 \\ \Delta t \end{bmatrix};$$

- u_t is the control input (g = -10 m/s$\hat{2}$) at time t;
- $\boldsymbol{\epsilon}_t$ is the process noise, modeled as $\mathcal{N}(\mathbf{0}, R)$.

Observation Models: Measurements are obtained from three sensor systems:

(i) GPS: The GPS sensor provides noisy measurements of the ball's position:

$$L_t = \begin{bmatrix} x_t^o \\ y_t^o \\ z_t^o \end{bmatrix} = C_t^{\text{GPS}}\,\mathbf{X}_t + \nu_t,$$

with

$$C_t^{\text{GPS}} = \begin{bmatrix} 1 & 0 & 0 & 0 & 0 & 0 \\ 0 & 1 & 0 & 0 & 0 & 0 \\ 0 & 0 & 1 & 0 & 0 & 0 \end{bmatrix},$$

and $\nu_t \sim \mathcal{N}(\mathbf{0}, Q_{\text{GPS}})$ denotes the measurement noise.

(ii) Base-Stations: The base stations are located at the four corners of the field at $z = 10$. Let their positions be denoted by $\mathbf{P}_i$ for $i = 1, \ldots, 4$. The measurements are the noisy distances from the ball to each base station:

$$D_t = \begin{bmatrix} D_{1t} \\ D_{2t} \\ D_{3t} \\ D_{4t} \end{bmatrix} = h(\mathbf{X}_t) + \delta_t,$$

where the nonlinear function $h(\cdot)$ is defined as

$$h(\mathbf{X}_t) = \begin{bmatrix} \|\mathbf{P}_1 - \mathbf{p}_t\| \\ \|\mathbf{P}_2 - \mathbf{p}_t\| \\ \|\mathbf{P}_3 - \mathbf{p}_t\| \\ \|\mathbf{P}_4 - \mathbf{p}_t\| \end{bmatrix}, \quad \text{with } \mathbf{p}_t = \begin{bmatrix} x_t \\ y_t \\ z_t \end{bmatrix},$$

and $\delta_t \sim \mathcal{N}(\mathbf{0}, Q_{\text{BS}})$ is the noise in the distance measurements.

(iii) IMU: The IMU provides noisy measurements of both the ball's position and velocity:

$$I_t = \begin{bmatrix} x_t^o \\ y_t^o \\ z_t^o \\ \dot{x}_t^o \\ \dot{y}_t^o \\ \dot{z}_t^o \end{bmatrix} = \mathbf{X}_t + \eta_t,$$

with $\eta_t \sim \mathcal{N}(\mathbf{0}, Q_{\text{IMU}})$ representing the measurement noise.

(b) Kalman/EKF Filters

To estimate the state of the ball, we employ filtering techniques that fuse the information from the above sensors.

For the linear models (GPS and IMU): A standard Kalman filter is applied. Let the state estimate at time $t-1$ be μ_{t-1} with error covariance Σ_{t-1}. Then:

Prediction:

$$\mu_{t|t-1} = A_t\, \mu_{t-1} + B_t\, u_t, \quad \Sigma_{t|t-1} = A_t\, \Sigma_{t-1}\, A_t^\top + R.$$

Update: When a measurement z_t is available with observation matrix C_t (either C_t^{GPS} or the identity matrix for the IMU),

$$\begin{aligned} K_t &= \Sigma_{t|t-1}\, C_t^\top \left(C_t\, \Sigma_{t|t-1}\, C_t^\top + Q\right)^{-1}, \\ \mu_t &= \mu_{t|t-1} + K_t \left(z_t - C_t\, \mu_{t|t-1}\right), \\ \Sigma_t &= (I - K_t\, C_t)\, \Sigma_{t|t-1}. \end{aligned}$$

For the nonlinear base-station measurements: Since the measurement function $h(\mathbf{X}_t)$ is nonlinear, an Extended Kalman Filter (EKF) is used. Let H_t be the Jacobian of h evaluated at the predicted state. Then the update step is modified as follows:

$$\begin{aligned} K_t &= \Sigma_{t|t-1}\, H_t^\top \left(H_t\, \Sigma_{t|t-1}\, H_t^\top + Q_{\text{BS}}\right)^{-1}, \\ \mu_t &= \mu_{t|t-1} + K_t \left(D_t - h(\mu_{t|t-1})\right), \\ \Sigma_t &= (I - K_t\, H_t)\, \Sigma_{t|t-1}. \end{aligned}$$

Jacobian of the Base-Station Observation Function: For the Extended Kalman Filter (EKF), we require the Jacobian of $h(\mathbf{X}_t)$ with respect to $\mathbf{X}_t$. Noting that $h(\mathbf{X}_t)$ depends only on the position components $\mathbf{p}_t = [x_t, y_t, z_t]^T$, the Jacobian matrix H_t is a 4×6 matrix given by

$$H_t = \frac{\partial h(\mathbf{X}_t)}{\partial \mathbf{X}_t} = \begin{bmatrix} \frac{\partial \|\mathbf{p}_t - \mathbf{D}_1\|}{\partial x_t} & \frac{\partial \|\mathbf{p}_t - \mathbf{D}_1\|}{\partial y_t} & \frac{\partial \|\mathbf{p}_t - \mathbf{D}_1\|}{\partial z_t} & 0 & 0 & 0 \\ \frac{\partial \|\mathbf{p}_t - \mathbf{D}_2\|}{\partial x_t} & \frac{\partial \|\mathbf{p}_t - \mathbf{D}_2\|}{\partial y_t} & \frac{\partial \|\mathbf{p}_t - \mathbf{D}_2\|}{\partial z_t} & 0 & 0 & 0 \\ \frac{\partial \|\mathbf{p}_t - \mathbf{D}_3\|}{\partial x_t} & \frac{\partial \|\mathbf{p}_t - \mathbf{D}_3\|}{\partial y_t} & \frac{\partial \|\mathbf{p}_t - \mathbf{D}_3\|}{\partial z_t} & 0 & 0 & 0 \\ \frac{\partial \|\mathbf{p}_t - \mathbf{D}_4\|}{\partial x_t} & \frac{\partial \|\mathbf{p}_t - \mathbf{D}_4\|}{\partial y_t} & \frac{\partial \|\mathbf{p}_t - \mathbf{D}_4\|}{\partial z_t} & 0 & 0 & 0 \end{bmatrix}.$$

Explicitly, if we let

$$r_i = \|\mathbf{p}_t - \mathbf{D}_i\| = \sqrt{(x_t - D_{i,x})^2 + (y_t - D_{i,y})^2 + (z_t - D_{i,z})^2},$$

for $i = 1, \ldots, 4$, then the partial derivatives are

$$\frac{\partial r_i}{\partial x_t} = \frac{x_t - D_{i,x}}{r_i}, \quad \frac{\partial r_i}{\partial y_t} = \frac{y_t - D_{i,y}}{r_i}, \quad \frac{\partial r_i}{\partial z_t} = \frac{z_t - D_{i,z}}{r_i}.$$

Thus, the Jacobian becomes

$$H_t = \begin{bmatrix} \frac{x_t - D_{1,x}}{r_1} & \frac{y_t - D_{1,y}}{r_1} & \frac{z_t - D_{1,z}}{r_1} & 0 & 0 & 0 \\ \frac{x_t - D_{2,x}}{r_2} & \frac{y_t - D_{2,y}}{r_2} & \frac{z_t - D_{2,z}}{r_2} & 0 & 0 & 0 \\ \frac{x_t - D_{3,x}}{r_3} & \frac{y_t - D_{3,y}}{r_3} & \frac{z_t - D_{3,z}}{r_3} & 0 & 0 & 0 \\ \frac{x_t - D_{4,x}}{r_4} & \frac{y_t - D_{4,y}}{r_4} & \frac{z_t - D_{4,z}}{r_4} & 0 & 0 & 0 \end{bmatrix}.$$

Plots of the trajectories (ground truth and estimates)

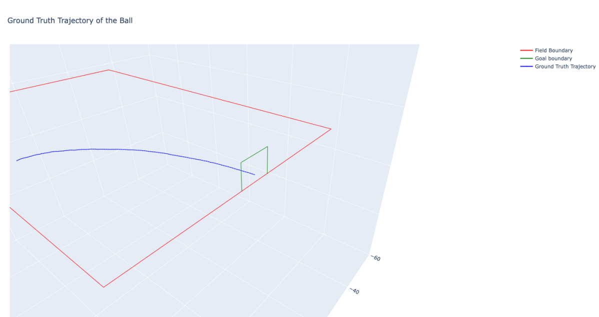

Figure 18: Ground Truth Trajectory

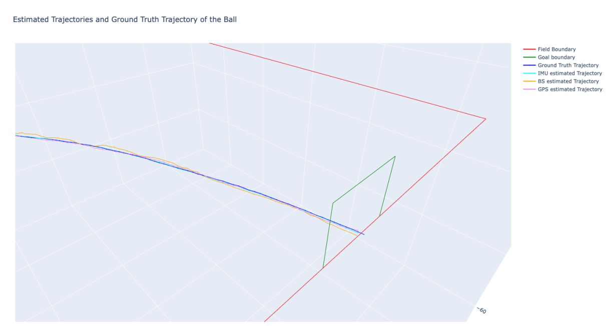

Figure 19: Ground Truth and all 3 Estimated Trajectories

We can see the estimates of the trajectories of all three system being close to the ground truth trajectory.

(c) Automated Refree System

Methodology for Automated Goal Detection

Our objective is to build an automated referee system to decide if a goal has been scored by a football.

The decision on whether a goal is scored is made by checking if the ball crosses the goal line within the goal region. The goal region is defined by:

$$-4 \leq x \leq 4, \quad 0 \leq z \leq 3, \quad \text{and} \quad y = 50.$$

(i) Decision Rule Using the Ground Truth Trajectory and Raw Data

When the ground truth trajectory is available, our decision rule is as follows:

- Compute the sequence of direction vectors between consecutive points:

$$\mathbf{d}_t = \mathbf{X}_{t+1} - \mathbf{X}_t, \quad t = 0, 1, \ldots, N-1.$$

- For each time step, check if the line segment between $\mathbf{X}_t$ and $\mathbf{X}_{t+1}$ crosses the plane $y = 50$. This is done by determining the scalar parameter α such that

$$y_t + \alpha\, d_{t,y} = 50.$$

- If $\alpha \in [0, 1]$ (or if the point itself lies on $y = 50$ in the boundary case), compute the corresponding x and z coordinates:

$$x^* = x_t + \alpha\, d_{t,x}, \quad z^* = z_t + \alpha\, d_{t,z}.$$

- Declare a goal if

$$x^* \in [-4, 4] \quad \text{and} \quad z^* \in [0, 3].$$

- In case final $y_t < 50$ then extrapolate the final coordinate in direction of d_{t-1} (edge case handling)

(ii) Decision Rule for Filtered Estimates

Filtering produces at each time step an estimate of the state in the form of a mean μ_t and covariance Σ_t. Because the filtered estimates include uncertainty, we extend our decision rule to account for this uncertainty:

- **Propagate:** We first propagate the estimates at $\mu_{\mathbf{t}}$ to $y = 50$ plane in direction of d_{t-1} like in previous method. Reason this is chosen as true trajectory has noise which takes $\mu_{\mathbf{t}}$ to $\mu_{\mathbf{t+1}}$, hence for propagation something that involves information from both points is considered important. Also propagate from point which is closer to $y = 50$ plane between $\mu_{\mathbf{t}}$ and $\mu_{\mathbf{t+1}}$.

- **Extracting the Position Component:** From the propagated state estimate, we consider the position in the x-z plane. Let

$$\mu_{\text{pos}} = \begin{bmatrix} \mu_x \\ \mu_z \end{bmatrix}, \quad \Sigma_{\text{pos}} = \begin{bmatrix} \Sigma_{xx} & \Sigma_{xz} \\ \Sigma_{zx} & \Sigma_{zz} \end{bmatrix}.$$

- **Constructing a Confidence Ellipse:** For a given confidence level (e.g., 95%), we compute the confidence ellipse defined by

$$\left\{ \mathbf{p} \in \mathbb{R}^2 : (\mathbf{p} - \mu_{\text{pos}})^\top \Sigma_{\text{pos}}^{-1} (\mathbf{p} - \mu_{\text{pos}}) \leq \chi^2_2(0.95) \right\}.$$

  This ellipse captures the uncertainty in the position estimate.

- **Decision Criterion:** At the time when the ball is predicted to cross the goal line (again determined by linear interpolation along the estimated trajectory), if the entire confidence ellipse is contained within the goal region

$$x \in [-4, 4] \quad \text{and} \quad z \in [0, 3],$$

  then we declare that a goal is scored.

We simulate 10000 trials and compute the fraction of estimates for which the decision rule declares a goal for with given noise values.

- Fraction of goals scored by ground truth: 0.2798
- Fraction of goals scored by GPS measurements: 0.2827

- Fraction of goals scored by IMU measurements: 0.2822
- Fraction of goals scored by GPS estimates: 0.2353
- Fraction of goals scored by BS estimates: 0.2092
- Fraction of goals scored by IMU estimates: 0.2461

(d) Varying noise parameters and analyzing Goals

We have described three types of noise parameters:

- Noise in the position update: σ_{pos} (with $\sigma_x = \sigma_y = \sigma_z$),
- Noise in the velocity update: σ_{vel} (with $\sigma_{\dot{x}} = \sigma_{\dot{y}} = \sigma_{\dot{z}}$), and
- Noise in the sensor measurements: σ_{GPS}.

For the GPS system, we repeat the goal detection experiment (as in part (c)) while varying each of the three noise parameters. Table **??** below summarizes the fraction of times a goal is scored, as determined by various methods (Ground Truth, GPS Measurement, IMU Measurement, BS Estimates, IMU Estimates, GPS Estimates) over 2000 simulations for different noise settings.

Table 1: Goal Scoring Simulation Results with Varying Noise Parameters (Selected Columns)

Index	σ_{pos}	σ_{vel}	σ_{GPS}	Ground Truth	GPS Measurement	GPS Estimates
0	0.0	0.0	0.01	0.9945	0.9865	0.9935
1	0.0	0.0	0.05	0.9965	0.7020	0.9840
2	0.0	0.0	0.1	0.9965	0.5190	0.9720
3	0.0	0.0	0.5	0.9970	0.4670	0.9985
4	0.0	0.0	1.0	0.9980	0.5715	1.0000
5	0.0	0.1	0.01	0.2775	0.2785	0.2700
6	0.0	0.1	0.05	0.2900	0.2890	0.2660
7	0.0	0.1	0.1	0.2840	0.2875	0.2375
8	0.0	0.1	0.5	0.2735	0.3255	0.1505
9	0.0	0.1	1.0	0.2900	0.4480	0.0995
10	0.0	0.2	0.01	0.2495	0.2515	0.2465
11	0.0	0.2	0.05	0.2530	0.2560	0.2405
12	0.0	0.2	0.1	0.2370	0.2335	0.2135
13	0.0	0.2	0.5	0.2590	0.2415	0.1605
14	0.0	0.2	1.0	0.2465	0.3030	0.1100
15	0.0	0.4	0.01	0.1630	0.1615	0.1605
16	0.0	0.4	0.05	0.1645	0.1605	0.1585
17	0.0	0.4	0.1	0.1490	0.1455	0.1330
18	0.0	0.4	0.5	0.1575	0.1315	0.0965
19	0.0	0.4	1.0	0.1590	0.1635	0.0650
20	0.0	0.8	0.01	0.0555	0.0555	0.0540
21	0.0	0.8	0.05	0.0670	0.0665	0.0600
22	0.0	0.8	0.1	0.0635	0.0610	0.0555
23	0.0	0.8	0.5	0.0560	0.0525	0.0365
24	0.0	0.8	1.0	0.0545	0.0700	0.0225
25	0.0	1.6	0.01	0.0225	0.0220	0.0215
26	0.0	1.6	0.05	0.0195	0.0170	0.0150
27	0.0	1.6	0.1	0.0170	0.0180	0.0145
28	0.0	1.6	0.5	0.0180	0.0150	0.0110
29	0.0	1.6	1.0	0.0265	0.0290	0.0065

Continued on next page

Table 1 (continued)

Index	σ_{pos}	σ_{vel}	σ_{GPS}	Ground Truth	GPS Measurement	GPS Estimates
30	0.01	0.0	0.01	0.4575	0.4585	0.3885
31	0.01	0.0	0.05	0.4450	0.4445	0.2455
32	0.01	0.0	0.1	0.4490	0.4145	0.1910
33	0.01	0.0	0.5	0.4370	0.4320	0.0185
34	0.01	0.0	1.0	0.4490	0.5500	0.0000
35	0.01	0.1	0.01	0.2985	0.2975	0.2930
36	0.01	0.1	0.05	0.2835	0.2775	0.2505
37	0.01	0.1	0.1	0.2645	0.2695	0.2275
38	0.01	0.1	0.5	0.2985	0.3415	0.1600
39	0.01	0.1	1.0	0.2820	0.4215	0.0920
40	0.01	0.2	0.01	0.2435	0.2450	0.2385
41	0.01	0.2	0.05	0.2315	0.2300	0.2100
42	0.01	0.2	0.1	0.2630	0.2580	0.2325
43	0.01	0.2	0.5	0.2470	0.2405	0.1635
44	0.01	0.2	1.0	0.2355	0.3065	0.0990
45	0.01	0.4	0.01	0.1550	0.1560	0.1510
46	0.01	0.4	0.05	0.1625	0.1600	0.1535
47	0.01	0.4	0.1	0.1735	0.1625	0.1555
48	0.01	0.4	0.5	0.1495	0.1425	0.0935
49	0.01	0.4	1.0	0.1645	0.1640	0.0745
50	0.01	0.8	0.01	0.0555	0.0560	0.0530
51	0.01	0.8	0.05	0.0545	0.0550	0.0475
52	0.01	0.8	0.1	0.0585	0.0565	0.0515
53	0.01	0.8	0.5	0.0580	0.0580	0.0355
54	0.01	0.8	1.0	0.0515	0.0635	0.0165
55	0.01	1.6	0.01	0.0170	0.0175	0.0175
56	0.01	1.6	0.05	0.0195	0.0190	0.0185
57	0.01	1.6	0.1	0.0245	0.0235	0.0195
58	0.01	1.6	0.5	0.0195	0.0240	0.0105
59	0.01	1.6	1.0	0.0180	0.0225	0.0050
60	0.05	0.0	0.01	0.2825	0.2840	0.2640
61	0.05	0.0	0.05	0.3040	0.3055	0.2300
62	0.05	0.0	0.1	0.2965	0.2995	0.1970
63	0.05	0.0	0.5	0.2975	0.3695	0.0895
64	0.05	0.0	1.0	0.2965	0.4980	0.0415
65	0.05	0.1	0.01	0.2655	0.2625	0.2535
66	0.05	0.1	0.05	0.2750	0.2740	0.2305
67	0.05	0.1	0.1	0.3035	0.3030	0.2340
68	0.05	0.1	0.5	0.2725	0.3230	0.1365
69	0.05	0.1	1.0	0.2760	0.4190	0.0885
70	0.05	0.2	0.01	0.2535	0.2525	0.2470
71	0.05	0.2	0.05	0.2415	0.2380	0.2165
72	0.05	0.2	0.1	0.2305	0.2275	0.1990
73	0.05	0.2	0.5	0.2565	0.2505	0.1555
74	0.05	0.2	1.0	0.2195	0.2685	0.0880
75	0.05	0.4	0.01	0.1525	0.1525	0.1500
76	0.05	0.4	0.05	0.1495	0.1490	0.1355
77	0.05	0.4	0.1	0.1735	0.1635	0.1400
78	0.05	0.4	0.5	0.1650	0.1385	0.0895
79	0.05	0.4	1.0	0.1630	0.1795	0.0635
80	0.05	0.8	0.01	0.0635	0.0645	0.0660
81	0.05	0.8	0.05	0.0640	0.0635	0.0600
82	0.05	0.8	0.1	0.0615	0.0550	0.0535

Continued on next page

Table 1 (continued)

Index	σ_{pos}	σ_{vel}	σ_{GPS}	Ground Truth	GPS Measurement	GPS Estimates
83	0.05	0.8	0.5	0.0685	0.0525	0.0415
84	0.05	0.8	1.0	0.0640	0.0695	0.0250
85	0.05	1.6	0.01	0.0185	0.0180	0.0185
86	0.05	1.6	0.05	0.0185	0.0210	0.0165
87	0.05	1.6	0.1	0.0210	0.0215	0.0185
88	0.05	1.6	0.5	0.0145	0.0140	0.0050
89	0.05	1.6	1.0	0.0205	0.0245	0.0045
90	1.0	0.0	0.01	0.0240	0.0240	0.0240
91	1.0	0.0	0.05	0.0230	0.0245	0.0220
92	1.0	0.0	0.1	0.0270	0.0290	0.0240
93	1.0	0.0	0.5	0.0330	0.0350	0.0085
94	1.0	0.0	1.0	0.0255	0.0320	0.0000
95	1.0	0.1	0.01	0.0290	0.0290	0.0270
96	1.0	0.1	0.05	0.0255	0.0250	0.0200
97	1.0	0.1	0.1	0.0260	0.0265	0.0215
98	1.0	0.1	0.5	0.0260	0.0265	0.0055
99	1.0	0.1	1.0	0.0270	0.0315	0.0000
100	1.0	0.2	0.01	0.0315	0.0315	0.0310
101	1.0	0.2	0.05	0.0255	0.0245	0.0205
102	1.0	0.2	0.1	0.0235	0.0245	0.0205
103	1.0	0.2	0.5	0.0240	0.0290	0.0060
104	1.0	0.2	1.0	0.0280	0.0380	0.0000
105	1.0	0.4	0.01	0.0260	0.0250	0.0250
106	1.0	0.4	0.05	0.0285	0.0280	0.0290
107	1.0	0.4	0.1	0.0275	0.0255	0.0215
108	1.0	0.4	0.5	0.0230	0.0220	0.0050
109	1.0	0.4	1.0	0.0280	0.0365	0.0000
110	1.0	0.8	0.01	0.0185	0.0175	0.0180
111	1.0	0.8	0.05	0.0195	0.0215	0.0170
112	1.0	0.8	0.1	0.0210	0.0220	0.0190
113	1.0	0.8	0.5	0.0245	0.0255	0.0055
114	1.0	0.8	1.0	0.0240	0.0300	0.0000
115	1.0	1.6	0.01	0.0140	0.0140	0.0110
116	1.0	1.6	0.05	0.0135	0.0130	0.0130
117	1.0	1.6	0.1	0.0150	0.0155	0.0105
118	1.0	1.6	0.5	0.0120	0.0130	0.0025
119	1.0	1.6	1.0	0.0135	0.0175	0.0000
120	2.0	0.0	0.01	0.0155	0.0155	0.0145
121	2.0	0.0	0.05	0.0140	0.0125	0.0095
122	2.0	0.0	0.1	0.0155	0.0140	0.0100
123	2.0	0.0	0.5	0.0125	0.0145	0.0015
124	2.0	0.0	1.0	0.0150	0.0160	0.0000
125	2.0	0.1	0.01	0.0120	0.0115	0.0085
126	2.0	0.1	0.05	0.0140	0.0140	0.0120
127	2.0	0.1	0.1	0.0150	0.0150	0.0130
128	2.0	0.1	0.5	0.0125	0.0125	0.0040
129	2.0	0.1	1.0	0.0175	0.0185	0.0000
130	2.0	0.2	0.01	0.0135	0.0135	0.0120
131	2.0	0.2	0.05	0.0140	0.0135	0.0130
132	2.0	0.2	0.1	0.0110	0.0100	0.0080
133	2.0	0.2	0.5	0.0120	0.0125	0.0045
134	2.0	0.2	1.0	0.0100	0.0140	0.0000
135	2.0	0.4	0.01	0.0110	0.0110	0.0115

Continued on next page

Table 1 (continued)

Index	σ_{pos}	σ_{vel}	σ_{GPS}	Ground Truth	GPS Measurement	GPS Estimates
136	2.0	0.4	0.05	0.0155	0.0150	0.0135
137	2.0	0.4	0.1	0.0135	0.0145	0.0120
138	2.0	0.4	0.5	0.0125	0.0125	0.0035
139	2.0	0.4	1.0	0.0115	0.0130	0.0000
140	2.0	0.8	0.01	0.0105	0.0105	0.0095
141	2.0	0.8	0.05	0.0125	0.0125	0.0120
142	2.0	0.8	0.1	0.0110	0.0120	0.0085
143	2.0	0.8	0.5	0.0140	0.0140	0.0030
144	2.0	0.8	1.0	0.0130	0.0170	0.0000
145	2.0	1.6	0.01	0.0105	0.0105	0.0090
146	2.0	1.6	0.05	0.0120	0.0115	0.0110
147	2.0	1.6	0.1	0.0130	0.0125	0.0095
148	2.0	1.6	0.5	0.0095	0.0110	0.0025
149	2.0	1.6	1.0	0.0145	0.0100	0.0000

Observations and Discussion

- **Impact of σ_{GPS}:** With $\sigma_{pos} = \sigma_{vel} = 0$, as σ_{GPS} increases from 0.01 to 1.0, the fraction of goals detected using raw GPS measurements declines noticeably, whereas the ground truth remains nearly ideal (close to 0.997 on average). This indicates that the measurement noise significantly affects the sensor output and at the same time out estimates are close to ground truth!.
- **Effect of Velocity Noise (σ_{vel}):** For fixed σ_{GPS}, an increase in σ_{vel} (with $\sigma_{pos} = 0$) degrades the performance of the GPS measurements as well as the filtered estimates. Higher velocity noise appears to reduce the reliability of the system's ability to accurately declare goals.
- **Combined Effects:** When both σ_{pos} and σ_{vel} are increased (for example, $\sigma_{pos} = 1.0$ or 2.0 and σ_{vel} at nonzero values), the overall goal detection performance (as seen in the GPS measurements and corresponding estimates) deteriorates further. The filtered estimates (GPS, BS, and IMU estimates) tend to be more robust than the raw sensor measurements, but their performance still declines under high noise conditions.
- **Summary:** The table demonstrates that while the ground truth trajectory is largely unaffected by sensor noise, the performance of the GPS system is highly sensitive to variations in both position and velocity noise, as well as the measurement noise. Filtering improves the accuracy of the estimates, but extreme noise levels still lead to a lower fraction of correctly declared goals.

(e) Varying position noise and GPS sensor noise, and analysing 2D projection

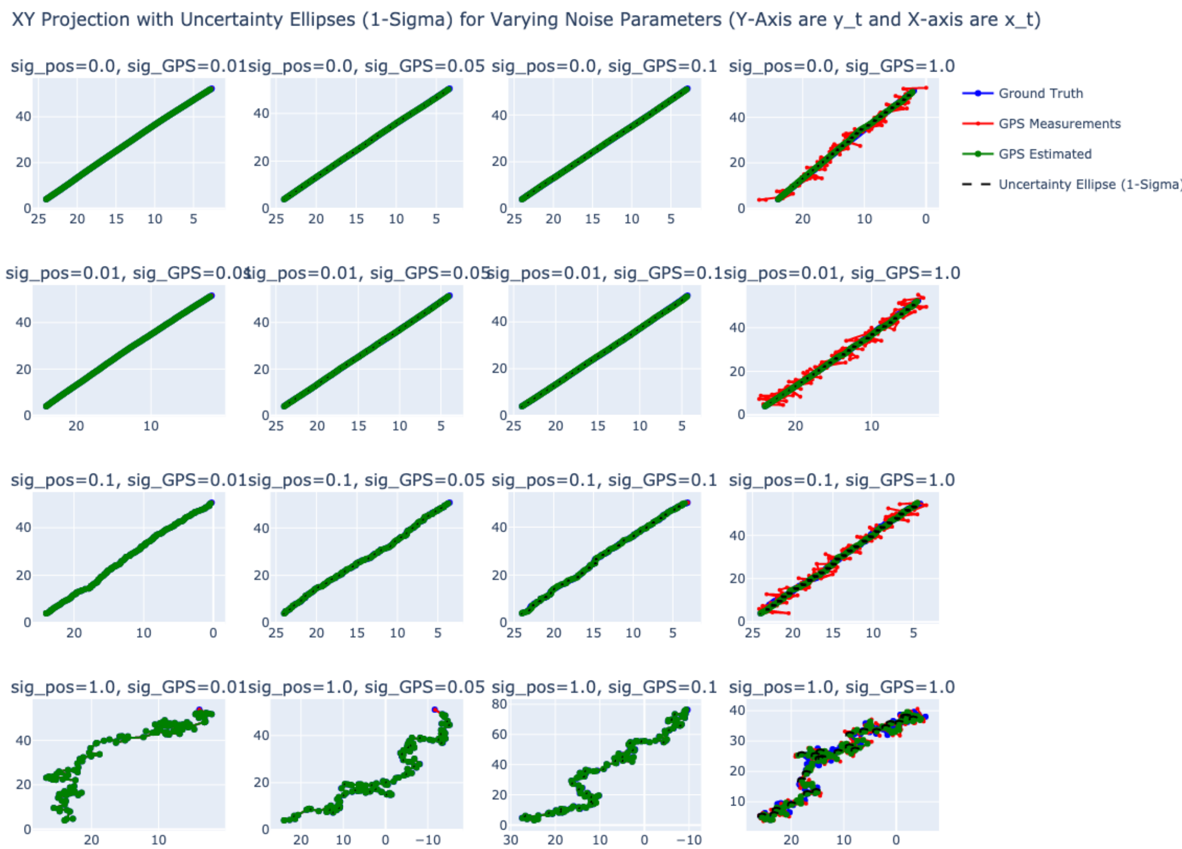

Figure 20: 2-D projections of trajectories with varying noise

Observations:

- As GPS noise is increased. the GPS measurements start to become fuzzy and uncertainity ellipses grow in size primarily in major axis. (observing graphs left to right).
- As position noise is increased, the trajectory starts to follow a much more random path (observing graphs from top to bottom) and uncertainity ellipse also grow in size primarily in major axis.

(f) New Simulation with 2D Trajectory and Uncertainty Ellipses

Plots of trajectories, uncertainty ellipses, major and minor axis

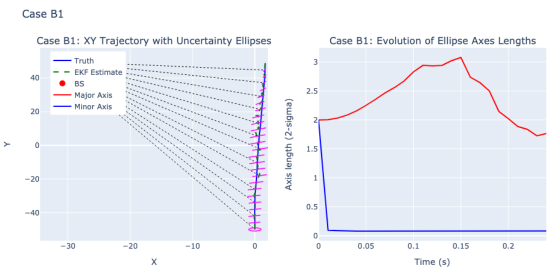

Figure 21: Case B1: 2D trajectory with uncertainty ellipse.

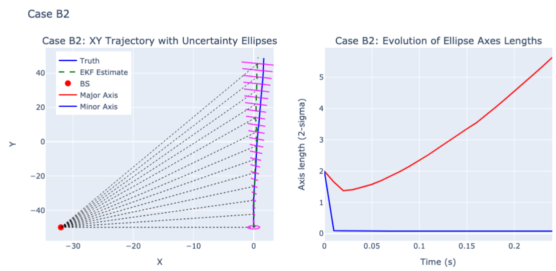

Figure 22: Case B2: 2D trajectory with uncertainty ellipse.

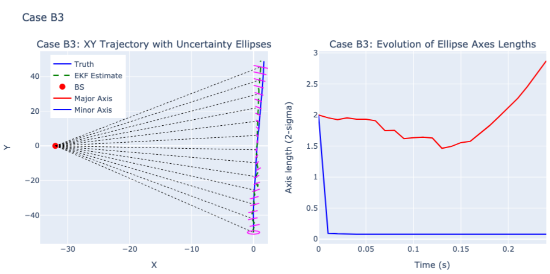

Figure 23: Case B3: 2D trajectory with uncertainty ellipse.

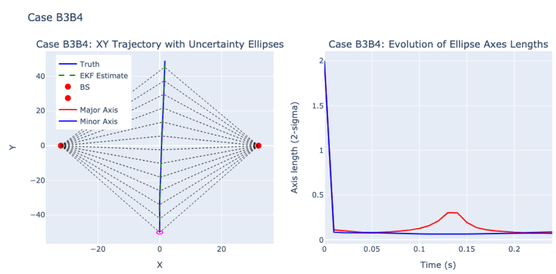

Figure 24: Case B3B4: 2D trajectory with combined uncertainty ellipses.

Base Station Geometry and Measurement Model

We now have four Base Stations (BS) with the following positions (in the XY plane):

- $B_1 = [-32, 50]$
- $B_2 = [-32, -50]$
- $B_3 = [-32, 0]$
- $B_4 = [32, 0]$

Each BS provides a noisy measurement of the Euclidean distance (with measurement noise standard deviation $\sigma_{BS} = 0.1$) from the ball to the BS. We consider observations from exactly one of the following cases:

1. Using measurements from B_1 only.
2. Using measurements from B_2 only.
3. Using measurements from B_3 only.
4. Using combined measurements from B_3 and B_4.

Orientation of the Uncertainty Ellipses

The uncertainty ellipses are derived from the 2×2 position covariance matrix. Their orientation is not arbitrary:

- When a BS provides a range (distance) measurement, it offers high information along the radial direction (i.e., along the line joining the BS and the ball) but little information in the tangential direction.
- As a result, the uncertainty is lower (the filter is more confident) in the radial direction and higher in the tangential direction. Thus, the ellipse tends to be elongated in the direction tangent to the line joining the BS and the ball.

As one can see in the plots, the lines from base stations to the ellipses indicate major axis of uncertainty ellipes being somewhat tangential (not tangential completely as covariance can provide some information in that direction).

In the case where measurements from two BSs (namely, B_3 and B_4) are combined, the geometry provides information from two distinct locations. This tends to reduce uncertainty in the direction perpendicular to the line joining the BSs, resulting in a more "rounded" (or less elongated) ellipse.

Major and Minor Axes of the Uncertainty Ellipses

At each time-step, we compute the lengths of the major and minor axes of the uncertainty ellipse (which are approximately given by twice the square-root of the eigenvalues of the position covariance matrix, corresponding to the 2σ spread).

- **Major Axis:** The direction along which the filter is less confident (i.e., the uncertainty is larger).
- **Minor Axis:** The direction along which the filter is more confident (i.e., the uncertainty is smaller).

Now Understanding the plots:

- **Minor Axis Across All Cases:** In all four scenarios, the minor axis length remains relatively small after the initial transient. This is because a range measurement from a single base station (or even two in a limited geometry) provides strong information in the radial direction (i.e., directly toward the base station). Consequently, the filter's uncertainty in that radial direction is kept low, which keeps the minor axis length small.
- **Case B1 (Base Station Away from the Starting Point):** The major axis length initially *rises* and then *falls*. Early in the trajectory, the filter has limited measurements, so the uncertainty in the tangential direction remains high, causing the major axis to grow. Over time, as the ball moves closer to the base station, each measurement update becomes more informative (the Jacobian's denominator is effectively smaller because the distance to the station is shorter). This stronger update reduces the tangential uncertainty, causing the major axis to decrease.
- **Case B2 (Base Station Close to the Starting Point):** Here, the major axis exhibits an initial *dip* before *increasing* again. At first, the ball is near the base station, so the range measurements provide strong updates and quickly reduce uncertainty, leading to the dip. However, as the ball moves farther away, the angle between the line from the base station to the ball and the ball's velocity increases. In this less favorable geometry, the filter struggles to reduce uncertainty in the tangential direction, so the major axis grows.
- **Case B3 (Base Station in the Middle of the Trajectory):** In this case, the major axis is minimized when the ball is near the base station (similar to Case B1 and B2 when ball is closer), but it grows as the ball moves away in either direction (similar to previous cases when ball is far). This results in a shape on the major axis plot that first decreases when the ball approaches the station, then increases again as the ball moves further away.

- **Case B3B4 (Two Opposite Base Stations in the Middle):** With two stations placed at opposite sides, the filter receives range measurements from two distinct angles, as such information two radial directions containing the velocity direction allow to reduce tangential uncertainty (bias towards sum of radial direction vectors from the base stations). As a result, the major axis length stays comparatively small throughout the simulation. A brief *peak* appear when the ball aligns with the line between B3 and B4, in this case the velocity direction being perpendicular to radial directions for both base stations suddenly increases uncertainity (as compared to earlier bias towards the sum of radial direction vectors is gone).